Synthesis and Characterization of Polyimide-γ-Fe_2O_3 Nanocomposites

H. V. Vijayanand,[1] L. Arunkumar,[1] P. M. Gurubasawaraj,[1] P. M. Veeresha Sharma,[1] S. Basavaraja,[1] A. Saleem,[1] A. Venkataraman,[1] Anil Ghanwat,[2] N. N. Maldar[2]

[1]*Department of Materials Science, Gulbarga University, Gulbarga, Karnataka, India*
[2]*Department of Chemistry, Sholapur University, Sholapur, Maharastra, India*

Received 6 January 2006; accepted 9 July 2006
DOI 10.1002/app.25186
Published online in Wiley InterScience (www.interscience.wiley.com).

ABSTRACT: Novel polyimide-γ-Fe_2O_3 hybrid nanocomposite films (PI/γ-Fe_2O_3) has been developed from the poly (amic acid) salt of oxydianiline with different weight percentages (5, 10, 15 wt %) of γ-Fe_2O_3 using tetrahydrofuran (THF) and *N*,*N*-dimethylacetamide (DMAc) as aprotic solvents. The prepared polyimide-γ-Fe_2O_3 nanocomposite films were characterized for their structure, morphology, and thermal behavior employing Fourier transform infrared spectroscopy (FTIR), scanning electron micrograph (SEM), transmission electron micrograph (TEM), X-ray diffraction (XRD), ^{13}C-NMR, and thermal analysis (TGA/DSC) techniques. These studies showed the homogenous dispersion of γ-Fe_2O_3 in the polyimide matrix with an increase in the thermal stability of the composite films on γ-Fe_2O_3 loadings. Magnetization measurements (magnetic hysteresis traces) have shown very high values of coercive force indicating their possible use in memory devices and in other related applications.
 J Appl Polym Sci 103: 834–840, 2007

Key words: γ-Fe_2O_3; magnetic polymers; nanocomposites; characterization studies

INTRODUCTION

Polyimides[1,2] are versatile high performance polymers that continue to gain importance in a wide variety of applications ranging from high temperature adhesives and composites, to microelectronics, membranes, and as photosensitive materials. These polymers have excellent thermal stability, high mechanical strength, good film-forming ability, superior radiation, chemical resistance, good adhesions, and low dielectric constant. However, their poor solubilities in common organic solvents and their infusibilities tend to limit their applications in many fields. Improved solubility can be achieved by incorporation of flexible groups into the polymer backbone to either reduce stiffness or lower the interchain interactions.[3–7] The range of topics covered and exploited by research demonstrates the continued interest in polyimides.

Polymer nanocomposites have emerged as a new class of materials in the last decade of the 20th century, which have attracted significant interest from researchers.[8,9] Polymer nanocomposites are materials in which nanoscopic inorganic particle, typically 10–100 nm in at least one dimension, are dispersed in an organic polymer matrix, to dramatically improve the performance properties of the polymer system. In addition, nanocomposites are usually transparent; because of the length scale of the particles that minimizes the scattering. Furthermore, the nanocomposites of polymer–metal oxide exhibit a significant increase in thermal stability as well as self-extinguishing characteristics. Advances in magnetic nanoparticles and polymer magnetic nanostructured technology have shown that some of these materials have the potential to play an important role in the diagnosis and treatment of cancer.[10] Among these materials, polyacrylamide magnetic iron oxide nanocomposites are employed as control agents for molecular imaging using MRI is reported.[11] Other interesting features have been observed when the polyimide has been loaded with magnetic materials[12] making them as polymer magnetic composites and these materials are supported to have applications as memory devices, magnetic fluids, and magnetic sensors, etc.[13] The urgent market demand to produce higher performance electronic devices with smaller size, light weight, and better quality developing polyimide (PI) films with low coefficient of thermal expansion has become one of the most important issue.[14,15] The reason for this behavior is that polyimide overcomes the thermal concentration and associated reliability problems produced by the mismatch between polymers, metals, and ceramics that make up electronic devices and enables polyimides to meet some ultimate requirement in the demanding applica-

Correspondence to: A. Venkataraman (raman_chem@rediffmail.com).

Contract grant sponsors: University Grants Commission (UGC), New Delhi, and Department of Science and Technology, Govt. of India.

tion. To date, one of the best ways to lower the CTE (coefficient of thermal expansion) is to incorporate inorganic materials such as γ-Fe_2O_3 into the polyimide matrix.[15] This paper is the continuation of our earlier work on γ-Fe_2O_3-polymer composites[16–19] to understand the effect of the loading of magnetic oxides and other additives in the polymer matrices. These studies showed interesting morphology, thermal and electrical behavior of the synthesized polymer composite films. The present investigation reports the effect (viz., structure, morphology, and thermal behavior) of the addition of different loadings of magnetic oxide, in the present case γ-Fe_2O_3, on polyimide matrix. The formation of polyimide is reported on the basis of FTIR and ^{13}C-NMR studies. Interesting magnetic properties like high coercivity and low saturation magnetization values with increasing weight percent of γ-Fe_2O_3 loadings were observed for these films, and this behavior predicts the possible applications for these composites as memory devices.

EXPERIMENTAL

All the chemicals were of AR grade and are used as received. Double distilled water was used for the preparation of the required solutions.

Purification of 3,3′,4,4′-benzophenone tetracarboxylic dianhydride

A known amount of benzophenone tetracarboxylic dianhydride (BTDA) was dissolved in distilled acetic anhydride and was heated till boiling, which was then cooled to get the crystals of BTDA. The crystals were then washed with dry benzene, followed by drying in vacuum at room temperature to remove moisture.

Preparation of polyimide

An Oxydianiline (0.005 mol, 1 g) of oxydianiline and 15 ml dimethylacetamide (DMAc) were mixed in a three-necked round-bottom flask maintained at 0°C, on a magnetic stirrer. The reaction mixture was then stirred in a dynamic flow of nitrogen atmosphere for an hour. To this reaction mixture, crystals of BTDA (0.005 mol, 1.61 g) were added 10 times with an interval of 10 min for further 2 h. A pale yellow viscous liquid of poly(amic acid) was formed. The possible mechanism of the formation of poly(amic acid) is depicted in Scheme 1.

Preparation of γ-Fe_2O_3 by microwave assisted route

The preparation procedure of the malonate precursor was adapted in our earlier report,[20] where equimolar

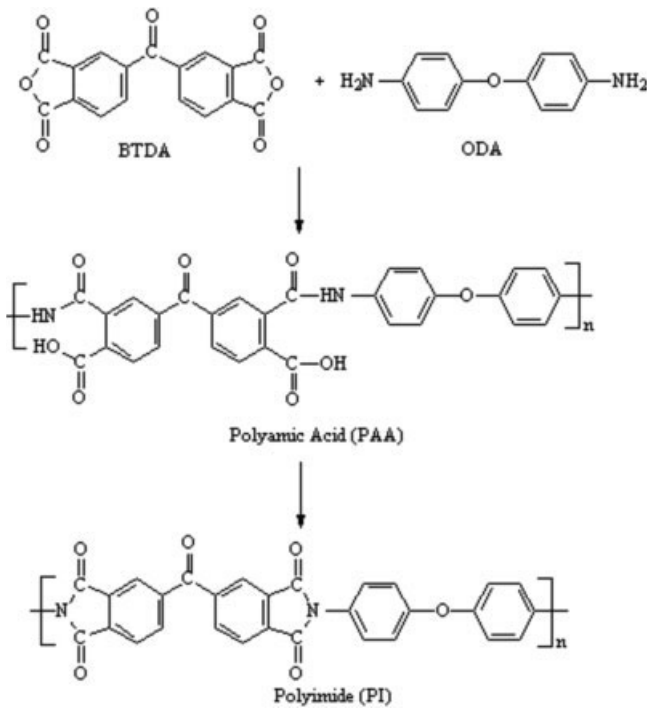

Scheme 1 Synthetic route to polyimide.

solution of ferrous ammonium sulfate hexahydrate was mixed with malonic acid placed on a magnetic stirrer, and the solution after adjusting to pH 7.0, was stirred for a few minutes. A light brown precipitate of ferrous malonate dihydrate was formed, which was filtered in a sintered crucible, washed with distilled water, and dried.

The above-prepared malonate precursor was heat-treated with polyvinyl alcohol (PVA) in a weight ratio of (1 : 5), in a silica crucible kept in an electrical oven. The evolution of voluminous gases takes place with the formation of a semicompleted reaction. The semicompleted reaction was then kept in a domestic microwave (of 2.45 GHz frequency) oven for 30 min (under low power conditions) when a brown colored magnetic powder was obtained. This brown powder was characterized as γ-Fe_2O_3 from structure and spectroscopic techniques. The morphology showed nanodimensions of the powder, which is explained in next section.

Preparation of polyimide-γ-Fe_2O_3 (PI-γ-Fe_2O_3) composite films

PI-γ-Fe_2O_3 composites were prepared with different weight percentages of γ-Fe_2O_3 (5, 10, and 15). The details of the method are as follows:

1 g of oxydianiline (ODA) and 1.61 g of benzophenone tetracarboxylic dianhydride (BTDA) in 15 mL of dimethyl acetamide gave viscous gel of 17.4% poly (amic acid), which was used for the experiment. Different weight percent of γ-Fe_2O_3 (5, 10, and 15 wt %) were sonicated for an hour and were added to the

weighed poly(amic acid), and the suspension was stirred for 2 h at room temperature under the flow of nitrogen. The composite films were then cast from the suspension placed on a glass plate kept in humid free chamber. The films henceforth are called as PI-γ-Fe_2O_3 films, with their weight ratios mentioned.

Characterization techniques

The infrared (IR) spectra of the samples were recorded on a PerkinElmer FTIR SpectrumONE in the range 4000–400 cm^{-1} at a resolution of 4 cm^{-1}. The ^{13}C-NMR spectra were recorded by DSX-300 FT-NMR spectrometer operated at 7.1 KHz. The XRD patterns were obtained with a Siemens X-ray diffractometer (Japan), and the target used was Cu Kα ($\lambda = 1.54$ Å). The generator was operated at 30 kV and with a 20 mA current. The scanning range (2θ) was selected from 5 to 80°. A scanning speed of 1°/min and a chart speed of 20 mm/min were used for the precise determination of the lattice parameters. The scanning electron micrograph (SEM) images of the samples were obtained with a JSM-840A scanning electron microscope. The scanning electron microscope was operated at 12 kV. The transmission electron micrograph (TEM) images and electron diffraction (ED) of the samples were obtained using Technai-20 Philips transmission electron microscope. The transmission electron microscope was operated at 190 KeV. Thermal data were obtained from Mettlar Toledo Star instruments (Weinheim, Germany) under a dynamic flow of nitrogen at a flow rate of 100 mL/min and a heating rate of 10°C/min. The magnetic hystereses of the samples were recorded at room temperature on a Magneta, Pulse field-magnetic hysteresis loop tracer.

RESULTS AND DISCUSSION

Fourier transform infrared spectroscopy study

The FTIR spectrum of the pure PI is shown in Figure 1(a). This figure shows the presence of aliphatic stretching frequencies at 2850–2890 cm^{-1}, symmetric imide frequency (C=O) at 1720–1730 cm^{-1}, asymmetric frequencies (C=O) stretching at 1790–1765 cm^{-1}, C—N bending at 730–760 cm^{-1} and typical poly(amic acid) absorption band at 3400–2900 cm^{-1} corresponds to amide (—NH—) and acid (OH) stretching. The (C=O) stretching frequencies of carboxylic acid at 1720 cm^{-1} and the (C—N) stretching frequencies of amide at 1540 cm^{-1} were not observed indicating the formation of polymer.

The IR spectrum of the PI-γ-Fe_2O_3 composite shown in Figure 1(b) had all the frequencies of Figure 1(a) with additional frequencies around 450 and 550 cm^{-1}, which correspond to the metal oxygen vibration frequencies of pure γ-Fe_2O_3.[21] There was a slight blue shift ($\approx$ 5 cm^{-1}) in these two peaks when compared with the pure γ-Fe_2O_3 (not shown in figure). This blue shift observed in the composite was possibly due to the weak bonding formed between PI and γ-Fe_2O_3.

^{13}C-NMR spectroscopy

Figure 2 shows solid-state NMR of the pure polyimide sample. The δ peaks observed at 180–210 ppm and 160–170 ppm are due to imide C=O and C—O bond, respectively. The broad peak at around 110–150 ppm was due to the aromatic region and the broadness of the peak confirms the formation of polymer. The peak at 20–40 ppm was due to some impurities present in the sample.

X-ray diffraction study

Figure 3(a–d) show the XRD patterns of pure polyimide and PI-γ-Fe_2O_3 composites.

The PI is amorphous as evident from XRD pattern (absence of any diffraction peaks) shown in Figure 3(a), while the XRD pattern of the γ-Fe_2O_3 (not shown) is polycrystalline with average particle size of 51.6 nm on calculating using the Scherer's formula for the FWHM of the maximum intensity peak (311),

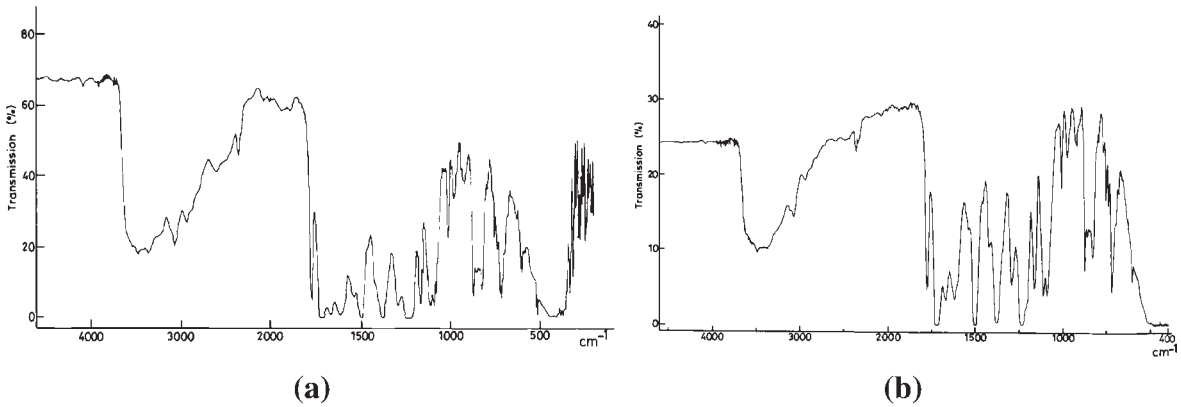

Figure 1 IR spectrum of (a) pure polyimide and (b) PI-γ-Fe_2O_3 sample.

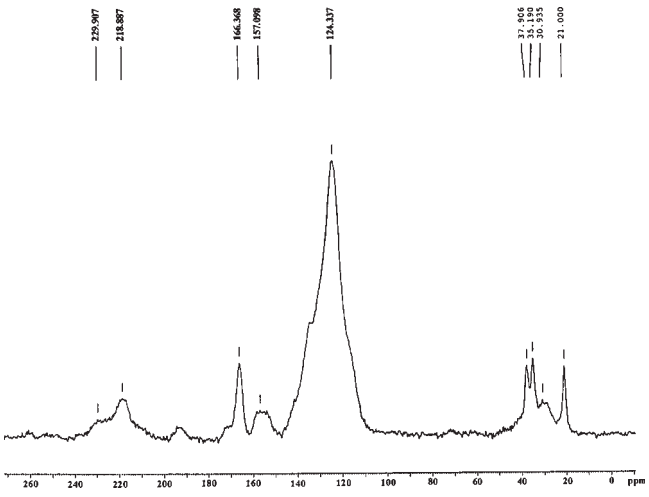

Figure 2 ^{13}C-NMR spectrum of polyimide.

indicating the nanodimension of the sample. Also, the TEM image along with the ED pattern for the γ-Fe_2O_3 is given at a later stage in this article for augmenting the explanation of the nanosize of this sample. Figure 3(b–d) showed the XRD pattern of PI-γ-Fe_2O_3 composites with different weight percentages of γ-Fe_2O_3 (5, 10, and 15%) respectively. On carefully observing the XRD patterns of these figures, it is understood that as the weight percent of γ-Fe_2O_3 increases, the crystalline nature of the composite also gets increased. In Figure 3(b), composites having 5 wt % shows less crystalline nature when compared with those having 10, which in turn is less crystalline than those having 15 wt %. The crystallite sizes of the 10 and 15 wt % composites are 38 and 44 nm respectively, when calculated by employing Scherer's formula for the (311) peak. These XRD pat-

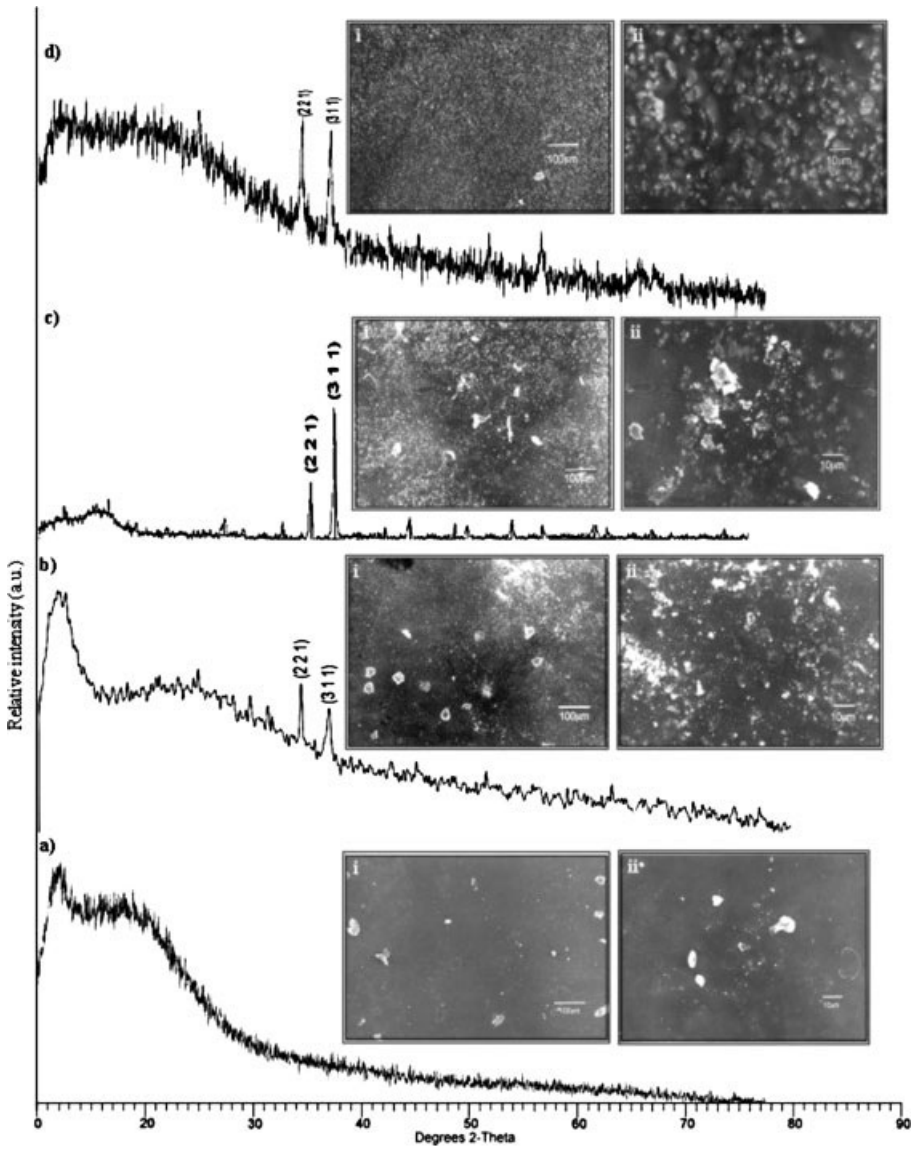

Figure 3 XRD pattern of pure polyimide and PI-γ-Fe_2O_3 composites of 5, 10, and 15 wt % (a–d), respectively and insets shows SEM images of the respective sample at low (i) and high magnification (ii).

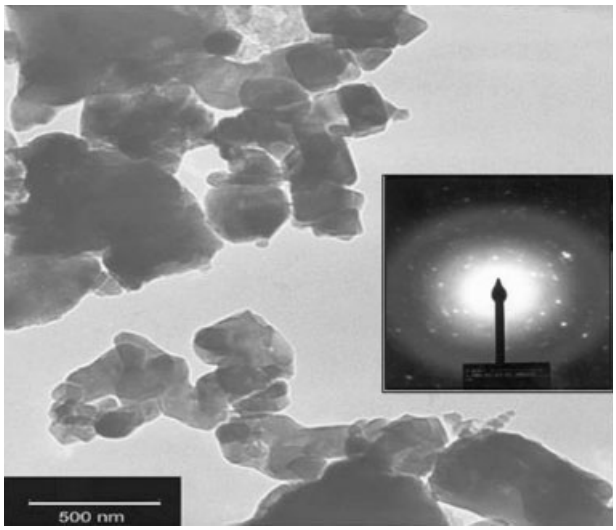

Figure 4 TEM image and ED pattern of γ-Fe_2O_3.

terns of the composites clearly indicate the change over from amorphous nature of the pure polymer to that of the partial crystalline state, when of γ-Fe_2O_3 particles are dispersed into the polymer matrix; this increase in the crystallinity of the polymer has also caused an increase in the thermal stability of the composite (discussed in the Thermal section of this article), and the changes in the morphology observed from the SEM and the TEM images discussed in the following sections.

Scanning electron micrograph study

The inset (i and ii) of Figure 3(a–d) shows the scanning electron micrograph images of the pure polyimide and PI-γ-Fe_2O_3 composites under low and high resolution respectively.

The inset (i and ii) of Figure 3(a) shows the SEM image of pure PI under low and high resolution respectively. The film shows some pores, which are usually observed due to some deformation of polymer film during casting.

The SEM images of PI-γ-Fe_2O_3 (5 wt % γ-Fe_2O_3) observed in Figure 3(b) showed particle agglomerates under both the resolutions. The agglomerates of the iron oxide particles appear to be submicron, while the average particles of the γ-Fe_2O_3 as mentioned earlier were nanosized. The low concentration of the oxide might have contributed to the particle agglomeration during film formation. Also, the dispersion of the oxide particles is not uniform, which again has been caused by its low concentration.

The inset (i and ii) of Figure 3(c) shows SEM image of PI-γ-Fe_2O_3 (10 wt % γ-Fe_2O_3). The dispersion looks more dense when compared with its predecessor (5 wt %); however, some submicron agglomerates are also noticed along with some pores of the original polymer film.

The SEM image of PI-γ-Fe_2O_3 (15 wt % γ-Fe_2O_3) shown as insert (i and ii) of Figure 3(d) had uniform dispersion of the iron oxide particles in the polymer even covering the pores observed in the polyimide film. The films look more homogenous; however, particle agglomerates cannot be ruled out in this case also.

From the SEM images it may be concluded that the higher percentage of γ-Fe_2O_3 up to 15 wt % loading shows better homogeneity and therefore may possess higher thermal stability.

Transmission electron micrograph

The nanocrystalline nature of the as prepared γ-Fe_2O_3 is further explained by bright field transmission electron micrograph (TEM) and electron diffraction pattern (ED) as insert is shown in Figure 4. TEM image shows the irregular shaped aggregate particles, which are closely joined. On careful observation, it is observed that these particles posses nanodimensions (< 100 nm in size). The electron diffraction pattern shows better resolution of the particles. The TEM image of the composite films could not be obtained because of experimental limitations.

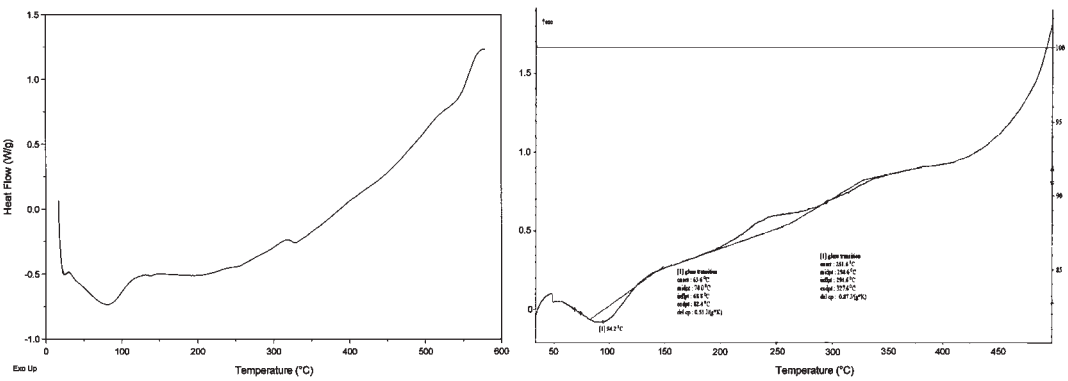

Figure 5 DSC trace of pure polyimide (a); TG and DSC traces of PI-γ-Fe_2O_3 sample (b).

Thermal analysis study

Figure 5(a, b) show the differential scanning calorimetry (DSC) traces for pure PI and DSC traces for 15 wt % γ-Fe_2O_3 loaded PI-γ-Fe_2O_3 respectively. Figure 5(a) shows a broad endothermic peak at around 85°C, which is due to the removal of hydrated water from the polymer. The small endothermic peak observed at 320°C corresponds to glass transition temperature of polyimide.

Figure 5(b) for the composite shows a broad endothermic peak at 94°C corresponds to the removal of hydrated water of composite. The glass transition temperature (T_g) was not clearly visible on the DSC trace; however, on close observation, the T_g was predicted at 327°C with the presence of a small endothermic peak. The increase in dehydration temperature from 85°C to 94°C and glass transition temperature by 7°C shows the increase in the thermal stability of the composite film.

Magnetic hysteresis study

Figure 6(a, c) show the magnetic hysteresis loop at room temperature for all the different weight percentage compositions of γ-Fe_2O_3 loaded into the polyimide matrix. The presence of magnetic hysteresis confirms the magnetic nature of the composites. The hysteresis loop shows very high values for coercivity when compared with the pure γ-Fe_2O_3 (H_c = 230 Oe and M_s = 52 emu/g, not shown in figure). The values of magnetic parameters of all the composite films are given in Table I.

The saturation magnetization values are higher for the 5 and the 15 wt % samples, whereas the coercivity is higher for the 10 wt % sample. These interesting results may be explained as follows:

The easy axis of magnetization for the γ-Fe_2O_3, i.e., along the (311) plane is freely oriented in 5 wt % of γ-Fe_2O_3 loading [Fig. 6(a)], whereas the same is restricted due to randomness of the γ-Fe_2O_3 grains oriented in different directions for 10 wt % [Fig. 6(b)] giving rise to lower M_s values. The increase in the amount of loading of γ-Fe_2O_3 particles might have contributed to this effect; however, the 10 wt % sample shows a square type hysteresis, an interesting feature (similar values of M_r and M_s), thereby indicating that this sample may have application in bubble memory devices. Figure 6(c) is interesting, as higher M_s value is observed. Possible reason for the

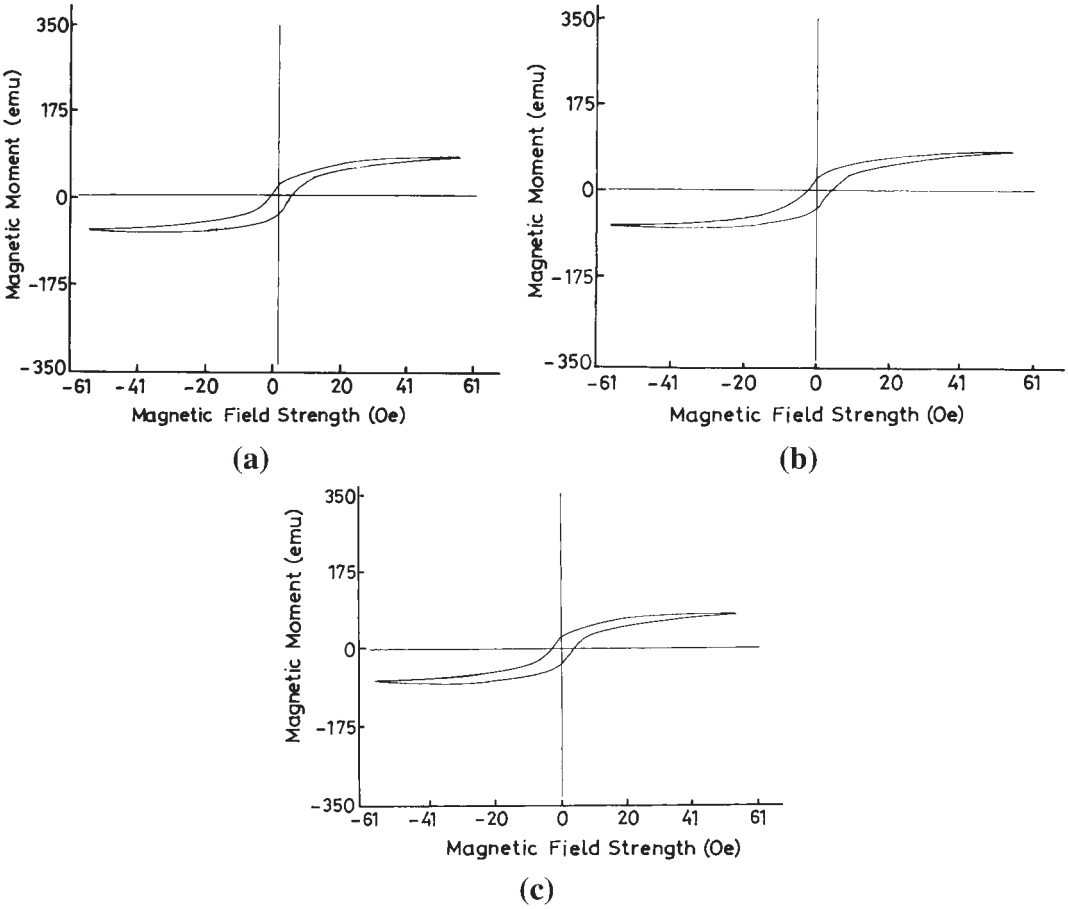

Figure 6 Magnetic hysteresis loop trace of (a) 5 wt %, (b) 10 wt %, (c) 15 wt % γ-Fe_2O_3 loaded PI-γ-Fe_2O_3 composite film.

TABLE I
Magnetic Properties of all the PI-γ-Fe_2O_3 Composite Films

Sample	H_c (Oe)	M_r (emu/g)	M_s (emu/g)
5 wt % γ-Fe_2O_3 loaded PI-γ-Fe_2O_3 composite film	400.20	0.20	2.87
10 wt % γ-Fe_2O_3 loaded PI-γ-Fe_2O_3 composite film	431.20	1.07	0.87
15 wt % γ-Fe_2O_3 loaded PI-γ-Fe_2O_3 composite film	380.00	0.20	3.40

higher value in this sample is attributed to the chemical homogeneity of the dispersed γ-Fe_2O_3 particles achieved in this film. It may also be mentioned here that the effect of particle size on magnetic behavior cannot be ruled out completely, though it is minimum in our case, as we have used the γ-Fe_2O_3 prepared in a single lot having almost similar morphology throughout. The coercivity values (H_c) also collaborate with the M_s values, as a ferromagnetic material generally increases as the hysteresis trace broadens (i.e., decreases in M_s values). However, the relationship between M_s and H_c is not mathematical. It may also be pointed out that the magnetic hysteresis traces and SEM images for our samples augment each other. On the basis of the magnetic hysteresis traces, we may conclude that the polymer matrix has hindered the free rotation of the easy axis of magnetization of γ-Fe_2O_3 particles in the composite film, thereby decreasing these M_s values, when compared with pure γ-Fe_2O_3. However, a very high increase in H_c values of the composite film, when compared with those of pure γ-Fe_2O_3, indicates the possible applications of there magnetic composite as memory devices and as magnetic memory sensors.

CONCLUSIONS

The method employed in the present study to synthesize PI-γ-Fe_2O_3 magnetic composite films shows increase in crystallinity and possess different morphology for different compositions, and better chemical homogeneity was observed for the composites with higher wt % of γ-Fe_2O_3 loading. An increase in the glass transition temperature of the composites when compared with the pure polymer (polyimide) indicated better dimensional and thermal stability of the processed films. The magnetic hysteresis results were interesting and also collaborate with the SEM images.

Part of the work was presented at the 16th Annual General Meeting of Materials Research Society of India-2005 held at National Chemical Laboratory, Pune, India, from 10th to 12th Feb. 2005.

References

1. Brydson, J. A. Plastic Materials, 7th ed.; Butterworth, 1999.
2. Parodi, F. Comprehensive Polymer Science Series, Vol. 5; Geoffrey, A. Ed.; Oxford University Press: New York, 1989.
3. Mark, H. F.; Bikales, N. M.; Overberger, C. G.; Menges Croschwitz, J. I. Encyclopedia of Polymer Science and Engineering, Vol. 12; Wiley: New York, 1988; p 363.
4. De Abajo, J.; De la Campa, J. G. In Handbook of Polymer Synthesis, 2nd ed.; Kricheldorf Oskar Nuyken, H. R.; Graham Swift, eds.; CRC Press: Boca Raton, FL, 2004.
5. Hallensleben M. L. In Handbook of Polymer Synthesis, 2nd ed.; Kricheldorf Oskar Nuyken, H. R., Graham Swift, eds.; CRC Press: Boca Raton, FL, 2004.
6. Mittal, K. I., ed. Polyimides: Synthesis, Characterization and Application, Vols. 1 and 2; Plenum: New York, 1984.
7. Feger, C.; Khojasteh, M. M.; Htoo, M. S., eds. Advances in Polyimide Science and Technology; Technimiun: Lancaster, PA, 1993.
8. Hasegawa, M.; Horie, K. Prog Polym Sci 2001, 26, 259.
9. Mallkpour, S. E.; Hajipour, A. R.; Fard, R. R. J Appl Polym Sci 2001, 79, 1716.
10. Koo, O. M.; Rubinstein, I.; Onyuksel, H. Nanomed Nanotechnol Biol Med 2005, 1, 193.
11. Moffat, B. A.; Ramachandra Reddy, G.; McConville, P.; Hall, D. E.; Chenevert, T. L.; Kopelman, R. R.; Philbert, M.; Weissleder, R.; Rehemtulla, A.; Ross B. D. Molecular Imaging 2003, 2, 324.
12. Yoon, C.; Sung Lim, K.; Kim, C. K.; Kim, Y.-H.; Yoon, C. S. J Magn Magn Mater 2004, 272–276, E1167.
13. Lim Sung, K.; Chung, K. J.; Kim, Y.-H.; Yoon, C. S. J Colloid Interface Sci 2004, 273, 517.
14. Chang, J.-H.; Park, K. M.; Lee, I. C. Polym Bull 2000, 45, 63.
15. Kim, Y. S.; Jund, J. C. Polym Bull 2000, 45, 311.
16. Govindaraj, B.; Sastry, N. V.; Venkataraman, A. J Appl Polym Sci 2004, 92, 1527.
17. Govindaraj, B.; Sastry, N. V.; Venkataraman, A. J Appl Polym Sci 2004, 93, 778.
18. Mallikarjuna, N. N.; Venkataraman, A.; Aminabhavi, T. M. J Appl Polym Sci 2004, 94, 2551.
19. Mallikarjuna, N. N.; Manohar, S. K.; Kulkarni, P. V.; Venkataraman, A.; Aminabhavi, T. M. J Appl Polym Sci 2005, 97, 1868.
20. Rahaman, M. M.; Mukhedkar, V. A.; Venkataraman, A.; Nikumbh, A. K.; Kulkarni, S. B.; Mukhedkar, A. J. Thermochimica Acta 1998, 125, 173.
21. Hiremath, A. V.; Venkataraman, A. Bull Mater Sci 2004, 26, 391.